Published in final edited form as:
ACS Chem Biol. 2014 February 21; 9(2): 423–432. doi:10.1021/cb400796c.

Multidimensional Profiling Platforms Reveal Metabolic Dysregulation caused by Organophosphorus Pesticides

Daniel Medina-Cleghorn[1], **Ann Heslin**[1], **Patrick J. Morris**[1], **Melinda M. Mulvihill**[1], and **Daniel K. Nomura**[1,*]

[1]Department of Nutritional Sciences and Toxicology, University of California, Berkeley, 127 Morgan Hall, Berkeley, CA 94720

Abstract

We are environmentally exposed to countless synthetic chemicals on a daily basis with an increasing number of these chemical exposures linked to adverse health effects. However, our understanding of the (patho)physiological effects of these chemicals remains poorly understood, due in-part to a general lack of effort to systematically and comprehensively identify the direct interactions of environmental chemicals with biological macromolecules in mammalian systems *in vivo*. Here, we have used functional chemoproteomic and metabolomic platforms to broadly identify direct enzyme targets that are inhibited by widely used organophosphorus (OP) pesticides *in vivo* in mice and to determine metabolic alterations that are caused by these chemicals. We find that these pesticides directly inhibit over 20 serine hydrolases *in vivo* leading to widespread disruptions in lipid metabolism. Through identifying direct biological targets of OP pesticides, we show heretofore unrecognized modes of toxicity that may be associated with these agents and underscore the utility of utilizing multidimensional profiling approaches to obtain a more complete understanding of toxicities associated with environmental chemicals.

Keywords

chlorpyrifos; activity-based protein profiling; metabolomics; organophosphate; pesticides; insecticides; chemoproteomics; serine hydrolase; proteomics; lysophosphatidic acid

Introduction

The large and continually increasing numbers of chemicals released into the environment necessitates a better understanding of their interactions with complex biological systems in order to predict and identify their toxicities and associated adverse health effects (1–3). Indeed, exposure to many chemicals in our environment such as pesticides, plasticizers, and flame retardants has been epidemiologically linked to human diseases (4–6), though their mode of action has often remained obscure, in-part due to the lack of knowledge surrounding the direct biological targets of these chemicals with specific protein targets *in vivo*. Current toxicology testing of chemicals employs toxicity assessments in animal models

*correspondence to dnomura@berkeley.edu.

Supporting Information Available: This material is available free of charge *via* the Internet.

or in cell or model organisms, genomic and proteomic assessment of transcriptional and protein expression changes, or testing chemical interactions with a small number of well-known toxicity targets (1, 3, 7). While these methods are powerful for identifying chemicals that cause well-established toxicities, elicit well-defined toxic transcriptional or protein expression changes, or interact with known toxic targets, these approaches are still lacking in their abilities to globally assess the functional targets of environmental chemicals on a proteome-wide scale. This challenge of uncovering the functional targets of environmental chemicals is further complicated by the majority of uncharacterized proteins in the mammalian genome, giving rise to large numbers of potential protein targets with unknown function and toxicities that are not assayed for under current testing paradigms. Understanding the toxicities associated with environmental chemicals could be greatly enhanced by employing strategies that facilitate a much broader assessment of the functional state of both well-understood and uncharacterized macromolecular targets *in vivo* to gain a comprehensive overview of chemical interactions with complex biological systems.

Over the past decade, functional chemical proteomic strategies have emerged as a powerful tool to broadly assess the functional state of the proteome and identify biological targets of small-molecules (8). One such chemoproteomic strategy termed activity-based protein profiling (ABPP) is a particularly powerful platform in which active-site directed chemical probes are used to broadly assess both characterized and uncharacterized enzyme activities *en masse* in complex biological systems (9–11). Because these activity-based probes bind to the active sites of whole classes of enzymes, small-molecules can be competed against probe binding to identify chemicals that alter protein function (9, 10, 12). Using ABPP platforms, we have previously identified functional targets of organophosphorus (OP) toxicants in mice and linked the inhibition of these targets to behavioral abnormalities, though our analyses were either limited to model OP compounds or low-content gel-based screens that provided restricted functional read-outs of enzyme activities (13–15).

In this study, we have combined ABPP and metabolomic platforms to more comprehensively identify and characterize both annotated and unannotated functional biological targets of several widely used organophosphorus (OP) pesticides *in vivo* across multiple tissues in mice. OP pesticides are used worldwide to control agricultural pests and crops (16, 17). Multiple studies have associated chronic human exposure to OP insecticides with a wide range of pathologies, including neurobehavioral deficits, developmental problems, obesity and diabetes, hormone level abnormalities, and lung cancer, but the mechanisms of action for these various health effects have remained obscure (18–24). Using ABPP and metabolomic platforms, we show here that these pesticides directly inhibit the activities of over 20 metabolic enzymes *in vivo* in mice at concentrations comparable to or lower than those required for inhibiting the primary toxicity target acetylcholinesterase (ACHE), leading to widespread alterations in lipid metabolism. We show that chemoproteomic and metabolomic approaches can be combined to more fully understand the biological effects associated with environmental chemicals, such as OP pesticides (Scheme 1).

Results and Discussion

Identification of OP Pesticide *in Vivo* Off-Targets in Mice using ABPP

In this study, we used ABPP to comprehensively identify all of the functional protein targets of several OP pesticides *in vivo* in mice. We focused our attention specifically on the serine hydrolase superfamily for profiling OP off-targets since previous studies have shown that the OP chemical scaffold is a privileged chemotype for this enzyme class (11, 25, 26). The serine hydrolase superfamily is a large class of metabolic enzymes that consists of lipases, esterases, hydrolases, thioesterases, proteases, and peptidases that play important (patho)physiological roles in nearly every biological setting (27). We used the activity-based probes for the serine hydrolase enzyme class, fluorophosphonate-rhodamine (FP-rhodamine) and FP-biotin, to detect a large number of serine hydrolase activities in mouse tissues by in-gel fluorescence or mass-spectrometry-based proteomics (ABPP-Multidimensional Protein Identification Technology (ABPP-MudPIT)), respectively (25).

We selected five pesticides for analysis by ABPP-MudPIT that we previously showed to be particularly promiscuous in inhibiting serine hydrolases—the OP insecticides chlorpyrifos (CPF), ethoprophos (EPP), and profenofos (PRF), the OP defoliant tribufos (TBF) and the thiocarbamate insecticide pebulate (PB) (Figure 1A) (13). Among these pesticides, CPF is currently the most widely used OP insecticide with 10 million pounds of active chemical annually applied in the U.S alone (17). To comprehensively determine any *in vivo* off-target interactions with serine hydrolases, mice were treated acutely for four hours with the maximum tolerated sublethal dose of each pesticide, brains were removed, and then brain proteomes were reacted with the FP-biotin serine hydrolase activity-based probe for subsequent avidin enrichment, tryptic digestion, and proteomic analysis (Scheme 1).

We find that each OP pesticide exhibits shared, as well as distinct serine hydrolase inhibitory profiles with CPF, EPF, and PRF each inhibiting 11, PB inhibiting 9, and TBF inhibiting 16 serine hydrolases out of 34 total serine hydrolase activities detected *in vivo* in mouse brain (Figure 1B, Table S1). Thus, our results strikingly show that OP pesticides block ~30–50 % of all serine hydrolase activities *in vivo* in the brain beyond ACHE. These inhibited targets include serine hydrolases monoacylglycerol lipase (MGLL) and fatty acid amide hydrolase (FAAH), acylpeptide hydrolase (APEH), KIAA1363, esterase 1 (ES1), carboxylesterase 1B (CES1B), hormone-sensitive lipase (LIPE), ACHE, alpha/beta hydrolase domain containing protein 3 (ABHD3), ABHD6, ABHD11, protein methylesterase 1 (PME1), lysophospholipase 2 (LYPLA2), and isoamylacetate hydrolase 1 (IAH1).

Inactivation of several of these enzymes have been linked to disease pathologies. Blockade of MGLL and FAAH, enzymes responsible for the breakdown of endogenous cannabinoid signaling lipids 2-arachidonylglycerol (C20:4 MAG) and anandamide (*N*-arachidonoylethanolamine, C20:4 NAE), respectively, have been shown to elicit cannabinoid receptor-mediated behaviors such as catalepsy, through the elevations in brain C20:4 MAG and C20:4 NAE (28). LIPE-deficient mice accumulate diacylglycerols and cholesteryl esters and exhibit male sterility and impaired corticosterone responses (29, 30). Mice deficient in the serine hydrolase KIAA1363, an acetyl monoalkylglycerol ether (2-

acetyl MAGe) hydrolase, show increased foam cell formation and aggravated atherosclerosis (31). Mice lacking both KIAA1363 and LIPE display aggravated atherosclerosis in an additive manner (31). ABHD3 hydrolyzes medium-chain and oxidatively truncated phospholipids (32). APEH has been shown to degrade monomeric and oligomeric amyloid-beta peptides (33). LYPLA2 has been shown to depalmitoylate proteins such as H-RAS and growth-associated protein-43 and alter their cellular localization (34). CPF also inhibits several uncharacterized serine hydrolases such as carboxylesterases (CES) CES1B and ES1, isoamylacetate-hydrolyzing esterase homolog 1 (IAH1), ABHD6, and ABHD11, which may cause yet unknown (patho)physiological responses.

Our results thus show that OP pesticides inhibit the activities of large number of serine hydrolases *in vivo* in mouse brain that play important roles in the metabolism of lipids and proteins and contribute to disease phenotypes when inactivated.

Identification of CPF Off-Targets in Peripheral Mouse Tissues *in Vivo*

We find that multiple enzymes such as MGLL, FAAH, ABHD3, APEH, and CES enzymes are inhibited in the brain as well as in peripheral tissues such as liver (Figure 1B), lung, testes, and kidney (Figure S1, Table S1, Supporting Information). We also report additional serine hydrolases not found in the brain that are blocked upon CPF-treatment in peripheral tissues, including arylacetamide deacetylase (AADAC), additional CES enzymes (CES1, CES1F, CES2, CES2B, CES2G, CES3, CES5, CES6, ES22), and butyrylcholinesterase (BChE) (Figure 1C, Figure S1, Table S1, Supporting Information). AADAC and CES enzymes have been implicated as triacylglycerol hydrolases. In particular, CES1-deficiency in mice has been shown to cause obesity, hepatic steatosis, and hyperlipidemia through controlling hepatic fat metabolism (35, 36). Collectively, our study reveals a staggering total of twenty-one metabolic serine hydrolases inhibited *in vivo* by CPF.

Assessing Potency of CPF Off-Targets

To validate our CPF *in vivo* targets, we comparatively assessed the inhibitory potency of the bioactivated form of CPF, chlorpyrifos-oxon (CPO), against either recombinantly expressed or native serine hydrolases in order to determine the relative inhibitory potency of CPO towards these off-targets compared to that of ACHE (Figure 1D). These results show that seven of the serine hydrolase off-targets have equivalent or lower 50 % inhibitory concentration (IC_{50}) values compared to that of ACHE (AADAC, HSL, CES1, CES2, MGLL, APEH, ABHD6), while four off-targets have IC_{50} values comparable to that of the ACHE IC_{50} (CES3, ABHD3, KIAA1363, FAAH) (Figure 1D). Among these targets, AADAC was the most sensitive target to CPO, showing a 28-fold lower IC_{50} of 0.6 nM, compared to 17 nM for ACHE. Many of the CPF off-targets may thus be inhibited at lower concentrations than those required to inhibit ACHE.

Metabolomic Profiling of CPF-Treated Mice Reveals Widespread Dysregulation of Lipid Metabolism

Many of the serine hydrolase off-targets inhibited by CPF have been previously characterized as possessing hydrolase activity towards both structural and signaling lipid substrates, suggesting that functional inhibition of serine hydrolases may alter lipid

metabolism *in vivo*. To comprehensively identify CPF-mediated alterations in lipid metabolism, we comparatively profiled the levels of ~150 lipids in mouse brain and liver of vehicle versus CPF-treated mice by targeted mass-spectrometry based metabolomics using single-reaction monitoring (SRM), and also compared the relative abundances of >10,000 ions by untargeted metabolomics (Scheme 1).

We observe widespread alterations in the lipidome of CPF-treated mouse brains and livers (Figure 2, Table S2, Supporting Information). In the brain, CPF treatment leads to elevations in the levels of neutral lipids monoacylglycerols (MAGs) and triacylglycerols (TAGs), N-acylethanolamines (NAE), sphingomyelin (SM), and the lysophospholipids lysophosphatidyl serine-ether (LPSe), C16:0, C18:0, and C18:1 lysophosphatidyl inositol (LPI), and C20:4 lysophosphatidic acid (LPA). We also find that CPF causes concurrent reductions in the levels of C20:4 free fatty acid (FFA) (arachidonic acid), acyl carnitines (ACs), monoalkylglycerol ether (MAGe), sphingosine-1-phosphate (S1P), and the lysophospholipids lysophosphatidic-ether (LPAe), C16:0 and C18:0 LPA, C20:4 LPI, and lysophosphatidyl choline (LPC) (Figure 2A, Table S2, Supporting Information). In the liver, CPF treatment leads to elevations in neutral lipids MAGs and DAGs, ACs, NAEs, SM, docosahexanoic acid (C22:6 FFA), N-acyl taurines (NATs) and phospholipids phosphatidyl inositol (PI), phosphatidyl inositol-ether (PIe), LPI, lysophosphatidyl inositol-ether (LPIe), and phosphatidyl choline-plasmalogen (PCp), and reductions in the levels of sphingosine, LPC, and phosphatidyl serine-ether (PSe) (Figure 2B, Table S2, Supporting Information).

Our results show that *in vivo* CPF inhibition of serine hydrolases causes widespread alterations in many classes of lipids spanning neutral lipids, phospholipids, fatty acids, ACs, NAEs, NATs, ether lipids, and sphingolipids. These changes include lipid signaling molecules such as the endocannabinoids C20:4 NAE and C20:4 MAG that act on cannabinoid receptors (37), LPA and LPAe that act on multiple Edg family of G-protein coupled LPA receptors as well as TRPV1 and GPR35 (38–41), S1P which also acts on multiple Edg family S1P receptors (38), NATs that are agonists for the TRPV1 channel (42), DAGs that can stimulate protein kinase C (43), and LPIs that stimulate GPR55 (44).

Many of the Metabolic Alterations are Directly Linked to Serine Hydrolase Off-Targets of CPF

We next sought to determine whether the CPF-induced lipidomic changes were a direct result of substrate accumulation or product depletion caused by inhibition of specific serine hydrolases. We performed a lipid hydrolysis screen on the metabolites we found to be elevated upon CPF-treatment, as these lipids may be substrates for CPF-inhibited serine hydrolases. Among the elevated lipids, we observed hydrolytic activity for C20:4 MAG, C20:4 NAE, C16:0e/C2:0 MAGe, C20:4 LPA, C16:0 LPI, and C20:4 NAT in mouse brain and liver. Among these lipids, C20:4 MAG, C20:4 NAE, C16:0e/C2:0 MAGe, C20:4 NAT, and C20:4 LPA hydrolytic activities were significantly inhibited in CPF-treated brain or liver proteomes (Figure 3A).

We attribute the CPF-induced elevations in MAGs in both brain and liver and C20:4 FFA depletion in brain and inhibition of C20:4 MAG hydrolytic activity to blockade of MGLL, based on previous studies with pharmacological or genetic inactivation of MGLL in mice

(45). Consistent with these previous studies, we show that MGLL hydrolyzes C20:4 MAG in MGLL-overexpressed in HEK293T cells (Figure 3B). The CPF-induced elevations in NAEs in brain and NAEs and NATs in liver and inhibition of NAE and NAT hydrolytic activity in brains or livers is attributable to inhibition of FAAH, based on previous metabolomic profiling of $FAAH^{-/-}$ mice (46). Consistent with these previous studies, we show that FAAH hydrolyzes C20:4 NAE and C20:4 NAT (Figure 3B). We attribute the CPF-induced lowering of MAGe levels and inhibition of C16:0e/C2:0 MAGe hydrolytic activity in the brain to inhibition of KIAA1363, based on previous studies with KIAA1363 inactivation in human cancer cells (47). We show that KIAA1363 indeed hydrolyzes C16:0e/C2:0 MAGe (Figure 3B).

The elevation in C16:0e/C2:0 MAGe in the liver and inhibition of C16:0e/C2:0 MAGe hydrolytic activity was intriguing to us, since we did not detect appreciable KIAA1363 activity in the liver by ABPP-MudPIT. However, AADAC shares 44 % identity with KIAA1363 in the liver, indicating that AADAC may control the levels and metabolism of C16:0e/C2:0 MAGe in the liver. Consistent with this premise, we show that AADAC, like KIAA1363, hydrolyzes C16:0e/C2:0 MAGe (Figure 3B).

Another interesting finding from our metabolomic profiling and lipid hydrolysis screen was an elevation in C20:4 LPA levels and inhibition of C20:4 FFA release from C20:4 LPA (Figure 3A), suggesting that one of the CPF-inhibited serine hydrolases may control the levels of C20:4 LPA in mouse brain. To identify this enzyme, we screened C20:4 LPA hydrolytic activity against CPF-off target serine hydrolases overexpressed in HEK293T cells. We surprisingly find that FAAH, MGLL, CES2, LIPE, ABHD3, CES1, and KIAA1363 are all capable of releasing C20:4 FFA from C20:4 LPA, with the highest activities attributed to MGLL and FAAH (Figure 3C, **first panel)**. We also show that MGLL blockade or MGLL/FAAH dual inhibition by the MGLL-selective inhibitor JZL184 or MGLL/FAAH-selective inhibitor JZL195, respectively, but not FAAH blockade alone by the FAAH-selective inhibitor PF3845, inhibits C20:4 LPA hydrolytic activity (Figure 3C, **second panel)**. These results indicate that C20:4 LPA may be hydrolyzed by MGLL. However, we also noticed substantial generation of C20:4 MAG from C20:4 LPA phosphatase activity, which was stabilized upon blockade of MGLL (Figure 3C, **third panel).** In light of this finding, we wanted to determine whether the apparent inhibition in C20:4 LPA hydrolytic activity was acting through MGLL directly acting on C20:4 LPA or through MGLL acting on the C20:4 MAG generated by dephosphorylation of C20:4 LPA. We thus performed the C20:4 LPA hydrolytic activity assay in the presence of phosphatase and phospholipase D inhibitors. Blockade of phosphatase activity significantly reduced the conversion of C20:4 LPA to C20:4 MAG (data not shown) and the apparent inhibition in C20:4 LPA hydrolytic activity with JZL184 was abolished (Figure 3C, **fourth panel)**, suggesting that C20:4 LPA is first dephosphorylated to generate C20:4 MAG which is in-turn hydrolyzed by MGLL.

Nonetheless, we were still intrigued by this connection between MGLL and C20:4 LPA and therefore tested whether $MGLL^{-/-}$ mouse brains had higher levels of this lipid. In addition to elevated C20:4 MAG and decreased C20:4 FFA levels reported previously (45), C20:4 LPA levels were significantly elevated by 2-fold in $MGLL^{-/-}$ brains compared to $MGLL^{+/+}$

counterparts, showing that MGLL controls the levels of this lipid in the brain, likely through heightened levels of C20:4 MAG undergoing phosphorylation to generate C20:4 LPA (Figure 3D).

LPA is a well-studied class of bioactive signaling lipids with significant roles in inflammation, nociception, and nervous system development, as well as in disease states such as metabolic diseases, cancer, and atherosclerosis (39, 41, 48–51). LPA signals through the LPA receptor family and has recently been shown to produce nociceptive effects through TRPV1 (38, 41). C20:4 LPA, in particular, has also recently been shown to be an agonist for the GPR35 receptor and GPR35 receptor signaling has been shown to modulate pain, metabolism, and inflammation (40). It will thus be of future interest to investigate the (patho)physiological consequence of CPF-induced elevations in brain levels of C20:4 LPA. Our findings show that MGLL may simultaneously control multiple signaling lipids in the brain, such as C20:4 LPA and C20:4 MAG that act through different receptor signaling pathways. Our finding gives rise to the possibility for cross-talk of these signaling lipids to coordinate the various phenotypic effects observed upon MGLL inactivation (28, 52, 53).

While we could not observe hydrolytic activities or inhibition of hydrolytic activities with the other lipids that were elevated in levels in CPF-treated mouse brain or liver under standard assay conditions, these alterations in the lipidome may still be linked to CPF-inhibited serine hydrolases either directly or indirectly. For example, diacylglycerol levels have been shown to be elevated in levels in LIPE-deficient mice (54), but we did not observe diacylglycerol hydrolytic activity in the brain. It will thus be of future interest to optimize hydrolytic assays for many of these lipids, such as LPI, DAG, and SM, to link CPF-induced lipidomic changes to CPF off-targets. Furthermore, the changes in these lipid species may also have (patho)physiological consequences. For example LPI and GPR55 signaling has been linked to pain, inflammation, and cancer (44).

Collectively, we show here that CPF blockade of MGLL, FAAH, KIAA1363, and AADAC lead to concordant changes in several classes of lipids (Figure 4A, B, and C). Additionally, we show that AADAC, like KIAA1363, is also a C16:0e/C2:0 MAGe hydrolase and that CPF blockade of AADAC may be responsible for the increased C16:0e/C20:0 MAGe levels in the liver. We also find that CPF elevates C20:4 LPA levels indirectly through MGLL blockade and phosphorylation of C20:4 MAG.

Summary

In this study, we find that OP pesticides disrupt the functions of multiple metabolic enzymes *in vivo* to exert alterations in lipid metabolism. Many of these enzymes, when inactivated, have been linked to various disease pathologies including neurobehavioral effects and metabolic disease. We show that several of these serine hydrolases are inhibited at CPO concentrations equivalent to or less than those required to inhibit ACHE, and may thus represent toxicological targets that may be responsible for the non-canonical toxicities associated with chronic OP pesticide exposure. For example, the cannabinoid-like behaviors that may result from CPF blockade of MGLL and FAAH and 2-AG and AEA elevations in brain may explain the neurobehavioral deficits associated with CPF exposure. The

obesogenic effects associated with CPF exposure may be through heightened endocannabinoid signaling or CES1 blockade.

Furthermore, using our coupled chemoproteomic and metabolomic approaches, we attribute novel functions to both AADAC as a C16:0e/C2:0 MAGe hydrolase and MGLL as an enzyme that indirectly controls brain C20:4 LPA levels. It will be of future interest to determine whether chronic and low-dose exposure to OP pesticides elicit many of the phenotypes associated with inactivation of the OP off-target serine hydrolases.

More broadly, we show here that employing multidimensional chemoproteomic and metabolomic profiling strategies facilitate a more comprehensive and deeper mechanistic understanding into potential toxicities that may be associated with chemical exposure by providing direct information on functional interactions of chemicals with proteins *in vivo*. We put forth that identifying direct functional targets of environmental chemicals provides information on the types of biological or toxicological effects that may be associated with chemical exposure and facilitates predictive toxicology assessment and may help to inform chemical design and ultimately improve chemical safety and human health (Scheme 1).

Methods

Mice

C57BL/6 male mice (6 weeks old) were exposed by intraperitoneal injection with each pesticide in a vehicle of 18:1:1 saline/emulphor/ethanol (10μl/g mouse). Animal experiments were conducted in accordance with the guidelines of the Institutional Animal Care and Use Committee of the University of California, Berkeley.

ABPP and Metabolomics

ABPP and metabolomic experiments were performed as previously described (55, 56). Details are outlined in Supplemental Methods.

Supplementary Material

Refer to Web version on PubMed Central for supplementary material.

Acknowledgments

We also thank C. Bertozzi and K. Collins of the University of California, Berkeley for use of their Typhoon flatbed scanners. This work was supported by the Searle Foundation, the Center for Environment Research on Toxics, and the National Institutes of Health (P42ES004705).

References

1. Bucher JR. Regulatory forum opinion piece: Tox21 and toxicologic pathology. Toxicol Pathol. 2013; 41:125–127. [PubMed: 22692375]
2. Huang RL, Xia MH, Cho MH, Sakamuru S, Shinn P, Houck KA, Dix DJ, Judson RS, Witt KL, Kavlock RJ, Tice RR, Austin CP. Chemical Genomics Profiling of Environmental Chemical Modulation of Human Nuclear Receptors. Environ Health Perspect. 2011; 119:1142–1148. [PubMed: 21543282]

3. Kavlock RJ, Austin CP, Tice RR. Toxicity testing in the 21st century: implications for human health risk assessment. Risk Anal. 2009; 29:485–487. discussion 492–487. [PubMed: 19076321]
4. Eskenazi B, Bradman A, Castorina R. Exposures of children to organophosphate pesticides and their potential adverse health effects. Environ Health Perspect. 1999; 107:409–419. [PubMed: 10346990]
5. Rochester JR. Bisphenol A and human health: A review of the literature. Reprod Toxicol. 2013; 42C:132–155. [PubMed: 23994667]
6. McDonald TA. A perspective on the potential health risks of PBDEs. Chemosphere. 2002; 46:745–755. [PubMed: 11999798]
7. Tice RR, Austin CP, Kavlock RJ, Bucher JR. Improving the human hazard characterization of chemicals: a Tox21 update. Environ Health Perspect. 2013; 121:756–765. [PubMed: 23603828]
8. Ziegler S, Pries V, Hedberg C, Waldmann H. Target Identification for Small Bioactive Molecules: Finding the Needle in the Haystack. Angewandte Chemie-International Edition. 2013; 52:2744–2792.
9. Nomura DK, Dix MM, Cravatt BF. Activity-based protein profiling for biochemical pathway discovery in cancer. Nat Rev Cancer. 2010; 10:630–638. [PubMed: 20703252]
10. Medina-Cleghorn D, Nomura DK. Chemical approaches to study metabolic networks. Pflugers Arch. 2013; 465:427–440. [PubMed: 23296751]
11. Evans MJ, Cravatt BF. Mechanism-based profiling of enzyme families. Chem Rev. 2006; 106:3279–3301. [PubMed: 16895328]
12. Moellering RE, Cravatt BF. How chemoproteomics can enable drug discovery and development. Chem Biol. 2012; 19:11–22. [PubMed: 22284350]
13. Nomura DK, Casida JE. Activity-based protein profiling of organophosphorus and thiocarbamate pesticides reveals multiple serine hydrolase targets in mouse brain. J Agric Food Chem. 2011; 59:2808–2815. [PubMed: 21341672]
14. Nomura DK, Blankman JL, Simon GM, Fujioka K, Issa RS, Ward AM, Cravatt BF, Casida JE. Activation of the endocannabinoid system by organophosphorus nerve agents. Nat Chem Biol. 2008; 4:373–378. [PubMed: 18438404]
15. Nomura DK, Leung D, Chiang KP, Quistad GB, Cravatt BF, Casida JE. A brain detoxifying enzyme for organophosphorus nerve poisons. Proc Natl Acad Sci U S A. 2005; 102:6195–6200. [PubMed: 15840715]
16. Casida JE, Durkin KA. Anticholinesterase insecticide retrospective. Chem Biol Interact. 2013; 203:221–225. [PubMed: 22926007]
17. Us Epa, O. o. P. P. Pesticides. US EPA; 2006–2007. Pesticide Market Estimates: Table of Contents (Sections).
18. Bouchard MF, Bellinger DC, Wright RO, Weisskopf MG. Attention-deficit/hyperactivity disorder and urinary metabolites of organophosphate pesticides. Pediatrics. 2010; 125:e1270–1277. [PubMed: 20478945]
19. Fortenberry GZ, Hu H, Turyk M, Barr DB, Meeker JD. Association between urinary 3, 5, 6-trichloro-2-pyridinol, a metabolite of chlorpyrifos and chlorpyrifos-methyl, and serum T4 and TSH in NHANES 1999–2002. Science of the Total Environment. 2012; 424:351–355. [PubMed: 22425279]
20. Rauh VA, Perera FP, Horton MK, Whyatt RM, Bansal R, Hao XJ, Liu J, Barr DB, Slotkin TA, Peterson BS. Brain anomalies in children exposed prenatally to a common organophosphate pesticide. Proceedings of the National Academy of Sciences of the United States of America. 2012; 109:7871–7876. [PubMed: 22547821]
21. Rauh VA, Garfinkel R, Perera FP, Andrews HF, Hoepner L, Barr DB, Whitehead R, Tang D, Whyatt RW. Impact of prenatal chlorpyrifos exposure on neurodevelopment in the first 3 years of life among inner-city children. Pediatrics. 2006; 118:E1845–E1859. [PubMed: 17116700]
22. Marks AR, Harley K, Bradman A, Kogut K, Barr DB, Johnson C, Calderon N, Eskenazi B. Organophosphate Pesticide Exposure and Attention in Young Mexican-American Children: The CHAMACOS Study. Environmental Health Perspectives. 2010; 118:1768–1774. [PubMed: 21126939]
23. Freire C, Koifman S. Pesticide exposure and Parkinson's disease: epidemiological evidence of association. Neurotoxicology. 2012; 33:947–971. [PubMed: 22627180]

24. Alavanja MCR, Dosemeci M, Samanic C, Lubin J, Lynch CF, Knott C, Barker J, Hoppin JA, Sandler DP, Coble J, Thomas K, Blair A. Pesticides and lung cancer risk in the agricultural health study cohort. American Journal of Epidemiology. 2004; 160:876–885. [PubMed: 15496540]
25. Bachovchin DA, Ji T, Li W, Simon GM, Blankman JL, Adibekian A, Hoover H, Niessen S, Cravatt BF. Superfamily-wide portrait of serine hydrolase inhibition achieved by library-versus-library screening. Proc Natl Acad Sci U S A. 2010; 107:20941–20946. [PubMed: 21084632]
26. Simon GM, Cravatt BF. Activity-based proteomics of enzyme superfamilies: serine hydrolases as a case study. J Biol Chem. 2010; 285:11051–11055. [PubMed: 20147750]
27. Long JZ, Cravatt BF. The metabolic serine hydrolases and their functions in mammalian physiology and disease. Chem Rev. 2011; 111:6022–6063. [PubMed: 21696217]
28. Long JZ, Nomura DK, Vann RE, Walentiny DM, Booker L, Jin X, Burston JJ, Sim-Selley LJ, Lichtman AH, Wiley JL, Cravatt BF. Dual blockade of FAAH and MAGL identifies behavioral processes regulated by endocannabinoid crosstalk in vivo. Proc Natl Acad Sci U S A. 2009; 106:20270–20275. [PubMed: 19918051]
29. Osuga J, Ishibashi S, Oka T, Yagyu H, Tozawa R, Fujimoto A, Shionoiri F, Yahagi N, Kraemer FB, Tsutsumi O, Yamada N. Targeted disruption of hormone-sensitive lipase results in male sterility and adipocyte hypertrophy, but not in obesity. Proc Natl Acad Sci U S A. 2000; 97:787–792. [PubMed: 10639158]
30. Li H, Brochu M, Wang SP, Rochdi L, Cote M, Mitchell G, Gallo-Payet N. Hormone-sensitive lipase deficiency in mice causes lipid storage in the adrenal cortex and impaired corticosterone response to corticotropin stimulation. Endocrinology. 2002; 143:3333–3340. [PubMed: 12193545]
31. Sekiya M, Osuga J, Nagashima S, Ohshiro T, Igarashi M, Okazaki H, Takahashi M, Tazoe F, Wada T, Ohta K, Takanashi M, Kumagai M, Nishi M, Takase S, Yahagi N, Yagyu H, Ohashi K, Nagai R, Kadowaki T, Furukawa Y, Ishibashi S. Ablation of neutral cholesterol ester hydrolase 1 accelerates atherosclerosis. Cell Metab. 2009; 10:219–228. [PubMed: 19723498]
32. Long JZ, Cisar JS, Milliken D, Niessen S, Wang C, Trauger SA, Siuzdak G, Cravatt BF. Metabolomics annotates ABHD3 as a physiologic regulator of medium-chain phospholipids. Nat Chem Biol. 2011; 7:763–765. [PubMed: 21926997]
33. Yamin R, Zhao C, O'Connor PB, McKee AC, Abraham CR. Acyl peptide hydrolase degrades monomeric and oligomeric amyloid-beta peptide. Mol Neurodegener. 2009; 4:33. [PubMed: 19627603]
34. Kong E, Peng S, Chandra G, Sarkar C, Zhang Z, Bagh MB, Mukherjee AB. Dynamic palmitoylation links cytosol-membrane shuttling of acyl-protein thioesterase-1 and acyl-protein thioesterase-2 with that of proto-oncogene H-ras product and growth-associated protein-43. J Biol Chem. 2013; 288:9112–9125. [PubMed: 23396970]
35. Quiroga AD, Li L, Trotzmuller M, Nelson R, Proctor SD, Kofeler H, Lehner R. Deficiency of carboxylesterase 1/esterase-x results in obesity, hepatic steatosis, and hyperlipidemia. Hepatology. 2012; 56:2188–2198. [PubMed: 22806626]
36. Lo V, Erickson B, Thomason-Hughes M, Ko KW, Dolinsky VW, Nelson R, Lehner R. Arylacetamide deacetylase attenuates fatty-acid-induced triacylglycerol accumulation in rat hepatoma cells. J Lipid Res. 2010; 51:368–377. [PubMed: 19654421]
37. Blankman JL, Cravatt BF. Chemical probes of endocannabinoid metabolism. Pharmacol Rev. 2013; 65:849–871. [PubMed: 23512546]
38. Im DS. Pharmacological tools for lysophospholipid GPCRs: development of agonists and antagonists for LPA and S1P receptors. Acta Pharmacol Sin. 2010; 31:1213–1222. [PubMed: 20729877]
39. Toman RE, Spiegel S. Lysophospholipid receptors in the nervous system. Neurochem Res. 2002; 27:619–627. [PubMed: 12374197]
40. Zhao PW, Abood ME. GPR55 and GPR35 and their relationship to cannabinoid and lysophospholipid receptors. Life Sciences. 2013; 92:453–457. [PubMed: 22820167]
41. Nieto-Posadas A, Picazo-Juarez G, Llorente I, Jara-Oseguera A, Morales-Lazaro S, Escalante-Alcalde D, Islas LD, Rosenbaum T. Lysophosphatidic acid directly activates TRPV1 through a C-terminal binding site. Nat Chem Biol. 2012; 8:78–85. [PubMed: 22101604]

42. Saghatelian A, McKinney MK, Bandell M, Patapoutian A, Cravatt BF. A FAAH-regulated class of N-acyl taurines that activates TRP ion channels. Biochemistry. 2006; 45:9007–9015. [PubMed: 16866345]
43. Wymann MP, Schneiter R. Lipid signalling in disease. Nat Rev Mol Cell Biol. 2008; 9:162–176. [PubMed: 18216772]
44. Henstridge CM, Balenga NA, Kargl J, Andradas C, Brown AJ, Irving A, Sanchez C, Waldhoer M. Minireview: recent developments in the physiology and pathology of the lysophosphatidylinositol-sensitive receptor GPR55. Mol Endocrinol. 2011; 25:1835–1848. [PubMed: 21964594]
45. Nomura DK, Morrison BE, Blankman JL, Long JZ, Kinsey SG, Marcondes MC, Ward AM, Hahn YK, Lichtman AH, Conti B, Cravatt BF. Endocannabinoid hydrolysis generates brain prostaglandins that promote neuroinflammation. Science. 2011; 334:809–813. [PubMed: 22021672]
46. Long JZ, LaCava M, Jin X, Cravatt BF. An anatomical and temporal portrait of physiological substrates for fatty acid amide hydrolase. J Lipid Res. 2011; 52:337–344. [PubMed: 21097653]
47. Chiang KP, Niessen S, Saghatelian A, Cravatt BF. An enzyme that regulates ether lipid signaling pathways in cancer annotated by multidimensional profiling. Chem Biol. 2006; 13:1041–1050. [PubMed: 17052608]
48. Park GY, Lee YG, Berdyshev E, Nyenhuis S, Du J, Fu P, Gorshkova IA, Li Y, Chung S, Karpurapu M, Deng J, Ranjan R, Xiao L, Jaffe HA, Corbridge SJ, Kelly EA, Jarjour NN, Chun J, Prestwich GD, Kaffe E, Ninou I, Aidinis V, Morris AJ, Smyth SS, Ackerman SJ, Natarajan V, Christman JW. Autotaxinproduction of Lysophosphatidic Acid Mediates Allergic Asthmatic Inflammation. Am J Respir Crit Care Med. 2013; 188:928–940. [PubMed: 24050723]
49. Anliker B, Choi JW, Lin ME, Gardell SE, Rivera RR, Kennedy G, Chun J. Lysophosphatidic acid (LPA) and its receptor, LPA, influence embryonic schwann cell migration, myelination, and cell-to-axon segregation. Glia. 2013; 61:2009–2022. [PubMed: 24115248]
50. Schober A, Siess W. Lysophosphatidic acid in atherosclerotic diseases. Br J Pharmacol. 2012; 167:465–482. [PubMed: 22568609]
51. Mills GB, Moolenaar WH. The emerging role of lysophosphatidic acid in cancer. Nat Rev Cancer. 2003; 3:582–591. [PubMed: 12894246]
52. Mulvihill MM, Nomura DK. Therapeutic potential of monoacylglycerol lipase inhibitors. Life Sci. 2013; 92:492–497. [PubMed: 23142242]
53. Schlosburg JE, Blankman JL, Long JZ, Nomura DK, Pan B, Kinsey SG, Nguyen PT, Ramesh D, Booker L, Burston JJ, Thomas EA, Selley DE, Sim-Selley LJ, Liu QS, Lichtman AH, Cravatt BF. Chronic monoacylglycerol lipase blockade causes functional antagonism of the endocannabinoid system. Nat Neurosci. 2010; 13:1113–1119. [PubMed: 20729846]
54. Haemmerle G, Zimmermann R, Hayn M, Theussl C, Waeg G, Wagner E, Sattler W, Magin TM, Wagner EF, Zechner R. Hormone-sensitive lipase deficiency in mice causes diglyceride accumulation in adipose tissue, muscle, and testis. J Biol Chem. 2002; 277:4806–4815. [PubMed: 11717312]
55. Nomura DK, Long JZ, Niessen S, Hoover HS, Ng SW, Cravatt BF. Monoacylglycerol lipase regulates a fatty acid network that promotes cancer pathogenesis. Cell. 2010; 140:49–61. [PubMed: 20079333]
56. Benjamin DI, Cozzo A, Ji X, Roberts LS, Louie SM, Mulvihill MM, Luo K, Nomura DK. Ether lipid generating enzyme AGPS alters the balance of structural and signaling lipids to fuel cancer pathogenicity. Proc Natl Acad Sci U S A. 2013; 110:14912–14917. [PubMed: 23980144]

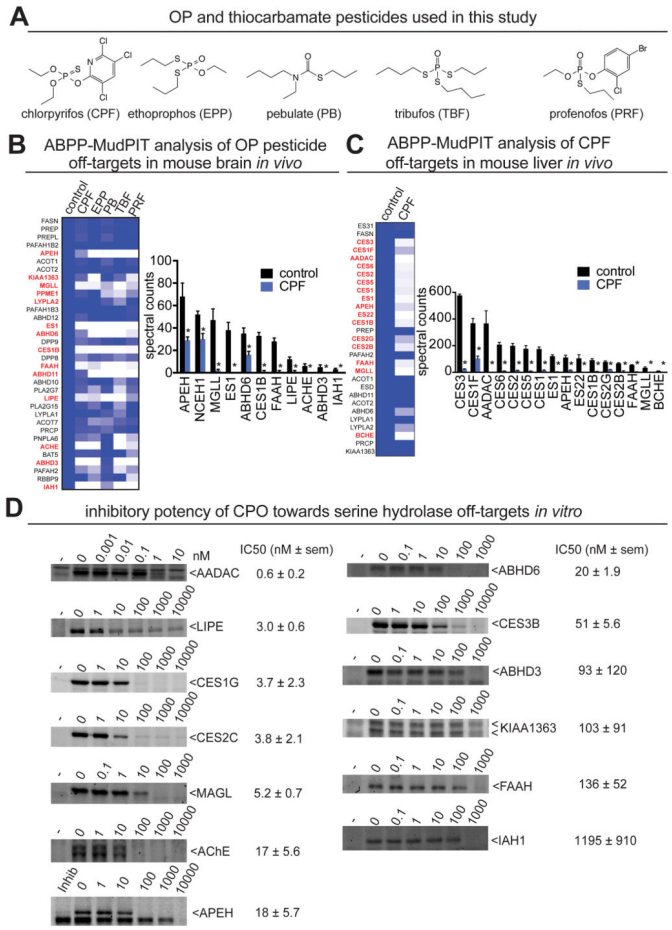

Figure 1. ABPP analysis of OP pesticides reveals large numbers of serine hydrolases inhibited *in vivo* in mice

(A) Structures of OP and thiocarbamate pesticides used in this study. (B, C) Competitive ABPP-MudPIT analysis of mouse brains (B) and livers (C) *ex vivo* from mice treated with OP and thiocarbamate pesticides CPF, EPF, PB, TBF, and PRF (50, 10, 100, 100, and 30 mg/kg ip, respectively, 4 h), shows multiple serine hydrolases that are inhibited *in vivo*. Brain and liver proteomes from control and pesticide-treated mice were treated with FP-biotin and active serine hydrolases were subsequently avidin-enriched and after subsequent processing, tryptic peptides were analyzed by LC-LC/MS/MS (MudPIT). Heat maps show all the serine hydrolases identified by ABPP-MudPIT. Darker blue shading on the heat map corresponds to high levels of activity, whereas lighter blue or white shading indicates lower activity. Serine hydrolases highlighted in red are significantly inhibited ($p<0.05$ compared to control) by one of the OP pesticides. Bar graphs show the significantly inhibited targets of CPF in brain (B) and liver (C). (D) The *in vitro* inhibitory potency of CPO against recombinantly overexpressed CPF off-target serine hydrolases. Serine hydrolases were individually expressed in HEK293T cells except APEH which was assayed directly in mouse brain proteomes. Lysates were pre-incubated with CPO then competitively labeled with FP-rhodamine and visualized by in-gel fluorescence. IC_{50}s were derived from densitometry based on gel-based ABPP analysis. Six off-target enzymes found in brain and liver are half-maximally inhibited (IC_{50}) at CPO concentrations between 1 and 26 times less

than required for CPF/CPO primary toxicity, inhibition of ACHE. Bar graphs in (B) and (C) and IC_{50} values in D are represented as mean ± SEM; n= 3–4 per group. Significance is expressed in *B* and *C* as $*p < 0.05$ compared with vehicle-treated controls.

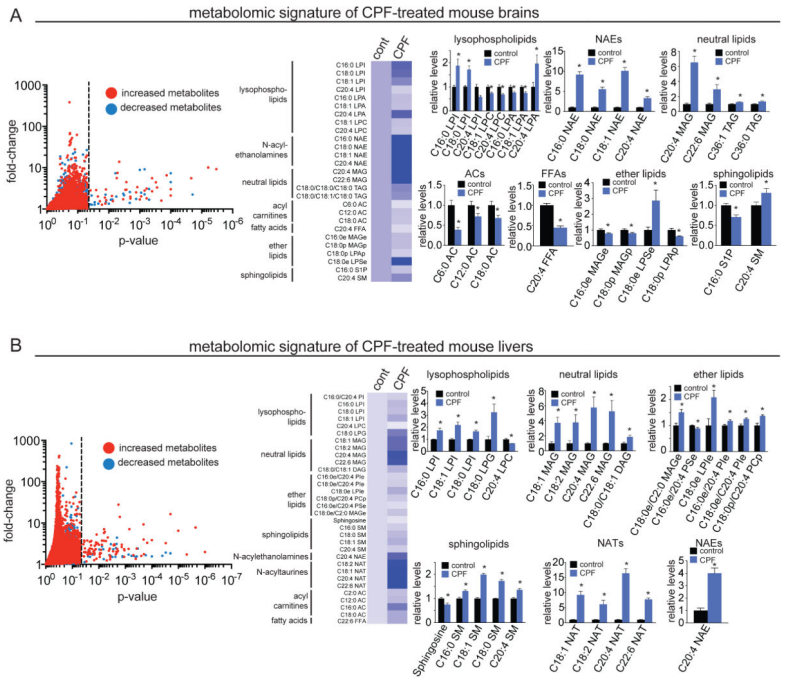

Figure 2. Metabolomic profiling of CPF-treated mice reveals widespread alterations in the mouse brain and liver lipidome

(A and B) Targeted and untargeted mass-spectrometry-based lipidomic profiling of brains (A) and livers (B) from mice treated with vehicle or CPF (50 mg/kg ip, 4 h). Left panel shows a volcano plot showing all the ions and metabolites detected by targeted and untargeted metabolomic profiling. Red and blue dots denote elevated and lowered metabolite levels in CPF-treated compared to vehicle-treated mice, respectively. Ions to the left ($p>0.05$) and right ($p<0.05$) of the dotted line are metabolites that are not significantly altered and significantly altered between vehicle versus CPF-treated mice, respectively. The heat map shows all identified metabolites in mouse brain that are significantly altered in response to CPF treatment. These metabolites were quantified by SRM-based targeted metabolomics and by untargeted metabolomics where putative identifications based on *m/z* and retention time were confirmed by analysis of a synthetic standard. Darker blue shading on the heat map corresponds to higher relative levels of metabolite, while lighter blue or white shading indicates lower relative abundance. Relative levels of lipids grouped by class are shown in bar graphs. Abbreviations for the lipid classes are as follows: PI, phosphatidyl inositol; LPI, lysophosphatidyl inositol; LPA, lysophosphatidic acid; LPC, lysophosphatidyl choline; LPG, lysophosphatidyl glycerol; NAE, N-acyl ethanolamine; NAT, N-acyltaurine; MAG, monoacylglycerol; DAG, diacylglycerol; TAG, triacylglycerol; AC, acyl carnitine; FFA, free fatty acid; MAGe, monoalkylglycerol ether; LPAp, lysophosphatidic acid plasmalogen; PSe, phosphatidyl serine ether; LPSe, lysophosphatidyl serine ether; S1P, sphingosine-1-phosphate; SM, sphingomyelin; PIe, phosphatidyl inositol ether; LPIe, lysophosphatidyl inositol ether, PCp, phosphatidyl choline plasmalogen;. Acyl or alkyl chain length is denoted as C(carbon length):(unsaturation). Raw data is presented in Table S2. Bar graphs in (A) and (B) are presented as mean ± SEM; n= 3–4 per group. Significance is

presented as *p< 0.05 comparing extracted lipid metabolome from CPF-treated and vehicle treated mice.

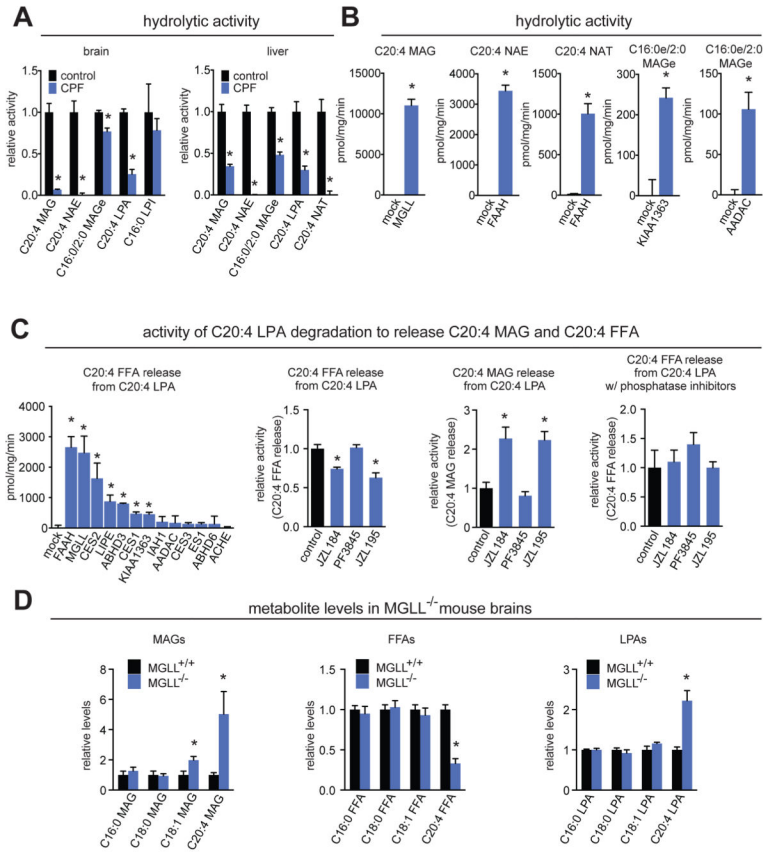

Figure 3. Several CPF-induced lipidomic alterations are linked to blockade of specific serine hydrolases

(A) Hydrolytic activities of lipids that are elevated upon CPF-treated mouse brains and livers assessed by quantitation of product formation by LC/MS. Lipids (100 μM, except C16:0 LPI at 10 μM) were incubated with vehicle- or CPF-treated (50 mg/kg ip, 4h) brain and liver proteomes for 30 min, 37°C. C20:4 FFA production was monitored for C20:4 MAG, C20:4 NAE, C20:4 NAT, and C20:4 LPA hydrolytic activity. C16:0 FFA production was monitored for C16:0 LPI hydrolytic activity. C16:0 MAGe production was monitored for C16:0e/C2:0 MAGe hydrolytic activity. (B) Hydrolytic activity of lipids in lysates from mock versus serine hydrolases-overexpressed in HEK293T cells. Lysates were incubated with lipids (100 μM, 10 μM C16:0 LPI) for 30 min at 37°C and product formation as assessed by LC/MS. (C) First panel shows C20:4 LPA hydrolytic activity (measured by C20:4 FFA release) in lysates from mock versus serine hydrolase-overexpressed HEK293T cells. Second and third panel shows C20:4 FFA and C20:4 MAG release, respectively, from C20:4 LPA hydrolysis or dephosphorylation in mouse brain proteomes pre-treated *in vitro* (1 μM, 30 min, 37°C) with DMSO, JZL184 (MGLL-selective inhibitor), PF3845 (FAAH-selective inhibitor), or JZL195 (MGLL/FAAH dual inhibitor). Fourth panel shows C20:4 FFA release from C20:4 LPA upon pre-incubation with 1 × protease/phosphatase inhibitor cocktail (Cell Signaling Technology) and 5-fluoro-2-indolyl des-chlorohalopermide (1 μM, phospholipase D inhibitor) for 15 min at 37°C prior to 30 min pre-incubation with selective inhibitors at 37°C and incubation with C20:4 LPA for 30 min at 37°C. (D) MAG, FFA, and LPA levels in mouse brains of $MGLL^{+/+}$ and $MGLL^{-/-}$ mice showing elevated levels of

C18:1 MAG, C20:4 MAG, C20:4 FFA, and C20:4 LPA. Data in (A–D) are presented as mean ± SEM; n= 3–4 per group. Significance is presented as * $p<0.05$ comparing CPF-treated, inhibitor-treated, or mock groups against vehicle-treated mice, control groups, or mock transfection in (A-C) and $MGLL^{-/-}$ compared to $MGLL^{+/+}$ mouse brain in (D).

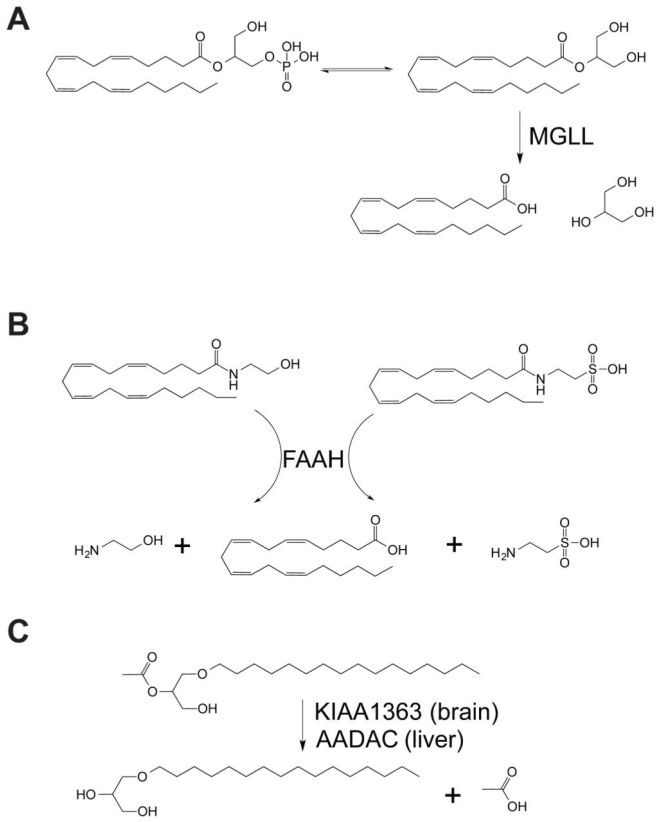

Figure 4. Metabolic pathways directed disrupted by CPF blockade of specific serine hydrolases

(A) CPF inhibits MGLL and leads to an accumulation of C20:4 MAG and lowering of C20:4 FFA levels with an indirect increase in C20:4 LPA, presumably through phosphorylation of C20:4 MAG. (B) CPF inhibits FAAH and leads to an accumulation in the levels of C20:4 NAE and C20:4 NAT. (C) CPF inhibits KIAA1363 in the brain and AADAC in the liver leading to lowered levels of MAGe in the brain and elevations C16:0e/C2:0 MAGe in the liver, respectively.

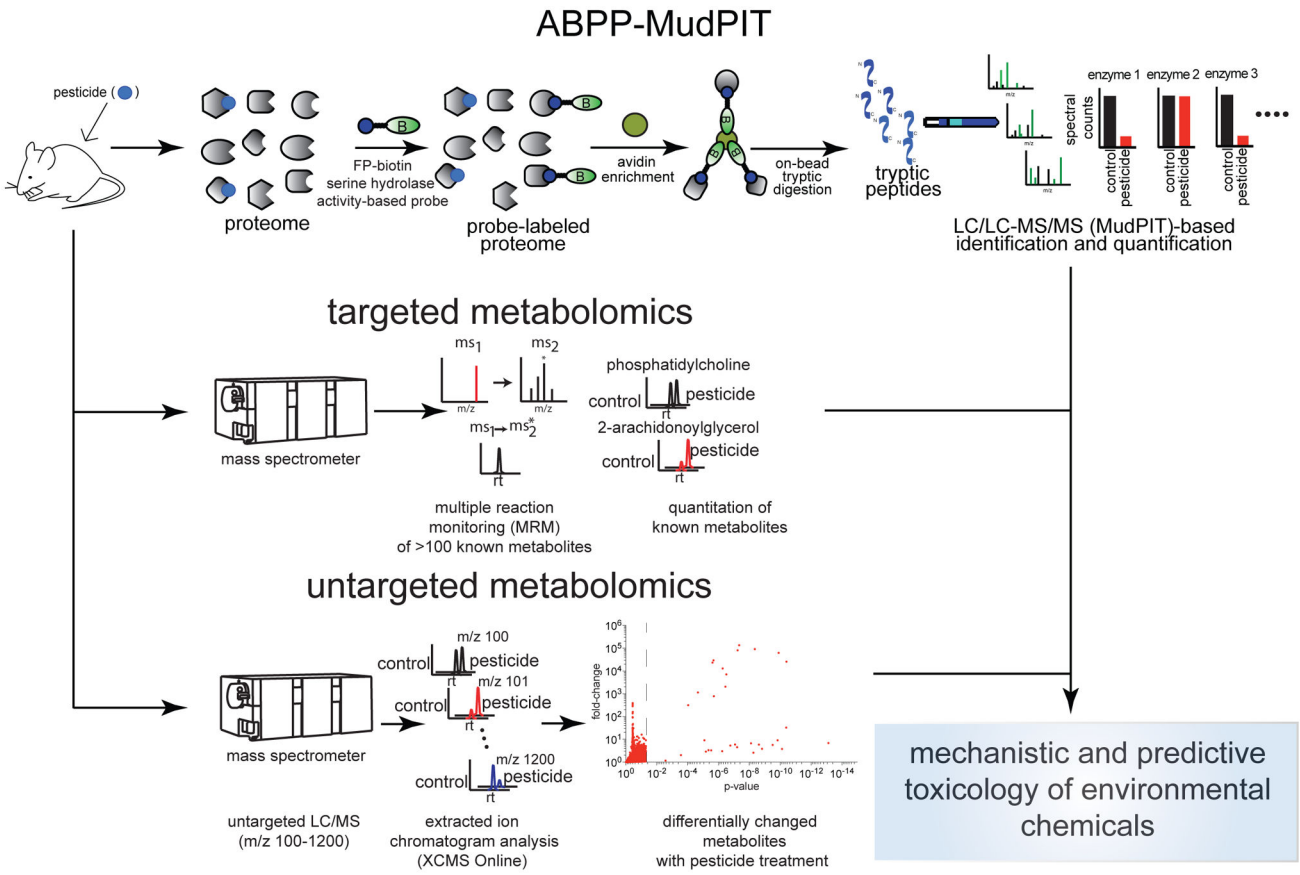

Scheme 1.